Environmental Science Nano

Surface Optimized Core-Shell Nanocomposites (Fe_3O_4@$Mn_xFe_yO_4$) for Ultra-High Uranium Sorption and Low-Field Separation in Water

Journal:	*Environmental Science: Nano*
Manuscript ID	EN-COM-07-2018-000826.R1
Article Type:	Communication
Date Submitted by the Author:	01-Sep-2018

Complete List of Authors:	Kim, Changwoo; Washington University in St. Louis, Energy, Environmental, and Chemical Engineering Lee, Seung Soo; Washington University in St. Louis, Energy, Environmental, and Chemical Engineering Reinhart, Benjamin; Argonne National Laboratory, X-Ray Sciences Division Cho, Minjung; Rice University, Chemistry; Houston Methodist, Translational Imaging Lafferty, Brandon; U.S. Army Corps of Engineers, Engineer Research and Development Center Li, Wenlu; Washington University in St. Louis, Department of Energy, Environmental & Chemical Engineering Fortner, John; Washington University in St. Louis, Energy, Environmental and Chemical Engineering

Surface Optimized Core-Shell Nanocomposites (Fe_3O_4@$MnFe_2O_4$) for Ultra-High Uranium Sorption and Low-Field Separation in Water

Changwoo Kim, [a,#] Seung Soo Lee, [a,#] Benjamin J. Reinhart,[b], [*a] Minjung Cho, [c] Brandon J. Lafferty, [d] Wenlu Li, [*a] and John D. Fortner [*a]

aDepartment of Energy, Environmental, and Chemical Engineering, Washington University, St. Louis, MO63130, USA.
bChemical Sciences and Engineering Division, Argonne National Laboratory, Lemont, IL 60439, USA
cDepartment of Translational Imaging and Department of Nanomedicine, Houston Methodist Research Institute, Houston, TX77030, USA
dEngineer Research and Development Center, US. Army Corps of Engineers, Vicksburg, MS39180, USA
# Authors contributed equally to this work
*Corresponding author: jfortner@wustl.edu

Environmental Significance Statement

Uranium separation and sensing in the environment remains a critical global challenge for environmental health. Herein, we describe a highly tunable core@shell type nanocrystal, which is unique in both approach (high flexible/tailorable) and high-performance regime(s) with regard to uranium sorption and separation. Taken together, demonstrated material properties underpin broad, platform potential for next generation water treatment, actinide separation and sensing technologies.

Journal Name

COMMUNICATION

www.rsc.org/

Surface Optimized Core-Shell Nanocomposites (Fe_3O_4@$Mn_xFe_yO_4$) for Ultra-High Uranium Sorption and Low-Field Separation in Water

Received 00th January 20xx,
Accepted 00th January 20xx

DOI: 10.1039/x0xx00000x

Changwoo Kim, [a,#] Seung Soo Lee, [a,#] Benjamin J. Reinhart,[b] Minjung Cho, [c] Brandon J. Lafferty, [d] Wenlu Li, *[a] and John D. Fortner *[a]

Multifunctional manganese ferrite coated superparamagnetic magnetite (core-shell) nanocrystals, surface stabilized by (organic) a phosphate functionalized bilayer, have been simultaneously optimized for ultra-high uranium sorption capacity, colloidal stability under elevated ionic strengths, and susceptibility to low magentic fields, which are critical for subsequent separation processes.

Superparamagnetic metal oxide nanocrystals (iron based materials such as, iron oxides, ferrites, etc.) have garnered significant interest for environmental applications due to their high potential in sorption, separation, sensing, and catalytic processes for a variety of aqueous pollutants including heavy metals and metalloids such as arsenic (As(III and V)), chromium (Cr(VI), and uranium (U(VI)).[1-7] A number of such materials have been developed by various wet chemical methods.[8-12] For example, Yavuz et al. demonstrated arsenic (As(III and V)) adsorption properties and magnetic separation of monodisperse iron oxide nanocrystals synthesized via a precise organic route.[10] Crane et al. reported the removal of U(VI) in water using iron oxide nanocrystals synthesized by coprecipitation method.[8] Dui et al. have demonstrated As(V) and Cr(VI) adsorption properties using $MnFe_2O_4$ hollow nanospheres ranging from 180 to 380 nm synthesized by a hydrothermal process.[9] Cai et al. have described a phosphorylated graphene oxide–chitosan composite for selective U(VI) removal.[11] Chen et al. reported amidoxime amended metal-organic framework for U(CI) extraction from seawater.[12]

Recently, our group has developed and demonstrated monodisperse manganese oxide (MO) and manganese ferrite (MF) nanocrystals with varying composition ratios of manganese to iron for ultra-high capacity uranium (VI) sorption and separation properties while considering colloidal stability, pH, and ionic strengths.[13] In these studies, iron-rich manganese ferrite ($MnFe_2O_4$) nanocrystals show better U(VI) sorption performance than manganese-rich manganese ferrite (Mn_2FeO_4) nanocrystals (q_{max} for $MnFe_2O_4$@OA and Mn_2FeO_4@OA at pH 7.0 was 667and 270 milligram of U per gram of nanocrystal (mg U / g NC), respectively). Higher concentration of Fe(II) (and Mn(II)) on the surface of $MnFe_2O_4$ leads to higher U(VI) sorption (than Mn_2FeO_4 materials) due to enhanced redox reactions between U(VI) and Fe(II) and Mn(II).[13]

Considering excellent uranium sorption by iron-rich manganese ferrite materials and the superparamagnetic properties of single domain iron oxides (IO), typically as magnetite, we propose that by combining these properties into one particle-based material – as a single domain magnetite core coated with a thin manganese ferrite – an optimized material for uranium sorption and separation may be achieved. Core@shell type biferrimagnetic nanocrystals have been synthesized as reported by López-Ortega and Krycka et al.[14] For these, iron oxide @ manganese ferrite (or manganese oxide) nanocrystals were synthesized under non-hydrolytic route by decomposing manganese (II) acetylacetonate (as a manganese precursor) with 1,2-hexadecandiol, oleylamine, and oleic acid in the presence of preformed iron oxide nanocrystals (as seed materials) at 200 ^oC.[14, 15] Resulting core@shell nanocrystals were shown to be manganese-rich $Mn_xFe_{3-x}O_4$ (in the range between Mn_3O_4 and Mn_2FeO_4) as the shell phase(s) on the surface of 11 nm iron oxide nanocrystals. However, based on our previous findings, iron-rich manganese ferrite surfaces are significantly better than manganese-rich ferrites with regard to U(VI) sorption capacities.

In this work, we have synthesized iron oxide nanocrystals coated with manganese ferrite (IO@MF) shells with varying composition ratios of manganese to iron (Figure 1). These nanocrystals were phase transferred into water via bilayer surface coatings, which consist of oleic acid (OA) inner layer and an oleylphosphate (OP), which has an outward facing

[a] Department of Energy, Environmental, and Chemical Engineering, Washington University, St. Louis, MO63130, USA. E-mail: wlib@wustl.edu; jfortner@wustl.edu
[b] Chemical Sciences and Engineering Division, Argonne National Laboratory, Lemont, IL 60439, USA
[c] Department of Translational Imaging and Department of Nanomedicine, Houston Methodist Research Institute, Houston, TX77030, USA
[d] Engineer Research and Development Center, US. Army Corps of Engineers, Vicksburg, MS39180, USA
# Authors contributed equally to this work
†Electronic Supplementary Information (ESI) available: See
DOI: 10.1039/x0xx00000x

phosphate head group. Uranium sorption was then explored and directly compared with analogous IO and MF particles with the same bilayer surface coatings.

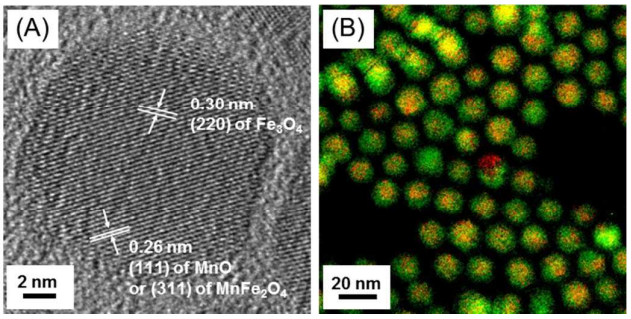

Fig 1. TEM images of the IO@MF nanocrystals. (A) HR TEM image of IO@MF nanocrystals. The lattice fringes of 0.30 nm (center) and 0.26 nm (side) correspond to (220) of Fe_3O_4 and (311) of $MnFe_2O_4$ (or (111) of MnO), respectively. (B) Gatan Image filter (GIF) image of IO@MF nanocrystals. The overlay map shows the distribution of iron (red) and manganese (green) in the particles.

Monodisperse, iron-rich manganese ferrite coated iron oxide nanocrystals (Fe-rich IO@MF) were precisely synthesized by decomposition of Mn-OA, as an Mn precursor, in the presence of preformed IO nanocrystal seeds in 1-octadecene at 320 ^{o}C for 1h. Shell composition control of the (i.e. Mn:Fe ratio) was achieved by precisely varying the molar ratio of Fe and Mn in the reaction (Fig S1).[14, 15] Specific synthetic processes are described in the SI. Average diameters of the resulting core@shell type nanocrystals increased slightly from 10.2 nm to 11.0 nm as a Mn-OA precursor decomposed onto the surface of seed materials (IO nanocrystal, d = 10.2 ± 0.9 nm) as shown in Fig S2.

Characterization of IO@MF materials is shown in Fig S3 and S4. Fe-rich manganese ferrite shell composition was observed with a molar ratio of Mn to Fe of 0.28 with no core alteration. Under these conditions, there was no evidence of forming individual (free) manganese oxide nanocrystals in the reaction as shown in GIF (Gatan Image Filter) images of the synthesized nanocrystals (Fig 1 and Fig S5). Furthermore, the composition ratio of Mn/Fe of the synthesized nanocrystal sample was identical with the ratio of Mn/Fe of the starting chemicals (the ratio of Mn-Ol/Fe-IO). As shown in Fig S6, XRD diffraction patterns of IO@MF nanocrystals with varied composition of Mn/Fe in an IO@MF nanocrystal from 0.28 to 0.73 are well matched to the diffraction patterns of magnetite (core, Fe_3O_4; red vertical lines; JCPDS cards #19-0629); however, MnO (200) phase was found from IO@MF with high ratio of Mn/Fe concentration over 2.1. A high ratio of Mn precursor to Fe seed material over 2.08 mol/mol led to the formation of manganese oxide layer(s) on the surface of IO seed materials.

The magnetic properties of engineered IO@MF nanocrystals were characterized by SQUID analysis (Fig 2). IO@MF, IO (Fe_3O_4), $MnFe_2O_4$, and Mn_2FeO_4 nanocrystals synthesized under organic reactions at 320^{o}C showed superparamagnetic behavior with hysteresis loops exhibiting nearly zero remanence and coercivity at 300K; 11 nm manganese oxide nanocrystals, which is known as core@shell type materials of MnO@Mn_3O_4 (antiferromagnetic core and ferrimagnetic shell) from the previous research, revealed a displacement of hysteresis loop along the magnetic field axis, exchange bias (H_E), with -274.6 Oe at 2K (Table S1).[13, 16] While being superparamagnetic, IO@MF nanocrystal samples were also similar to inverted soft/hard ferrimagnetic core@shell structures, exhibiting a higher exchange bias with -20.65 Oe of H_E at 2K (Table S1).[14, 15]

For aqueous application, we employed a surface-based organic bilayer technique to facilitate aqueous transfer and stability (Supplemental Information†).[13, 17] Oleylphosphate (OP) was used as a phase transfer agent (also as a surface stabilizer), which coordinates with the first surface layer (oleic acid) on the as-synthesized IO@MF nanocrystal surface via hydrophobic-hydrophobic interaction.[13, 17] The resulting hydrodynamic diameter (D_H) and surface charge for the phase transferred IO@MF@OP nanocrystals were 20.9 ± 3.0 nm with -50.4 ± 1.4 mV. These IO@MF@OP nanocrystals were also colloidally stable in water under relatively high ionic strengths. Critical coagulation concentration (CCC) values of sodium (Na) and calcium (Ca) for the particles were 892.5 mM of Na^+ and 15.9 mM of Ca^{2+} for IO@MF@OP (Fig S7).

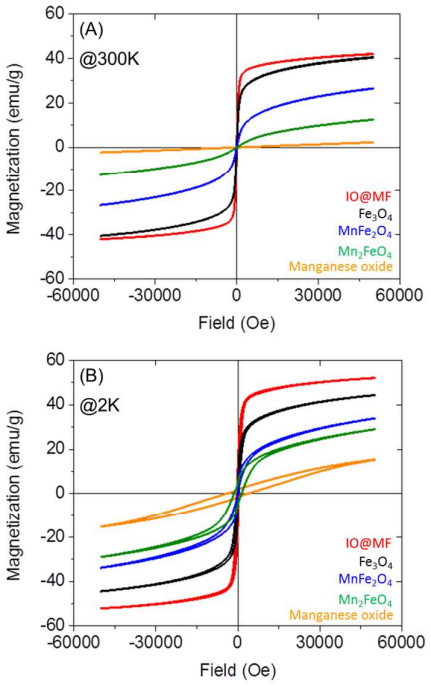

Fig 2. Magnetic properties of the nanoparticles synthesized under organic route. (A) Hysteresis curves of IO@MF ([Mn]/[Fe] = 0.28, red), Fe_3O_4 (black), $MnFe_2O_4$ (blue), Mn_2FeO_4 (green), manganese oxide (orange) measured at 300 K. (B) Hysteresis curves of IO@MF ([Mn]/[Fe] = 0.28, red), Fe_3O_4 (black), $MnFe_2O_4$ (blue), Mn_2FeO_4 (green), manganese oxide (orange) measured at 2K.

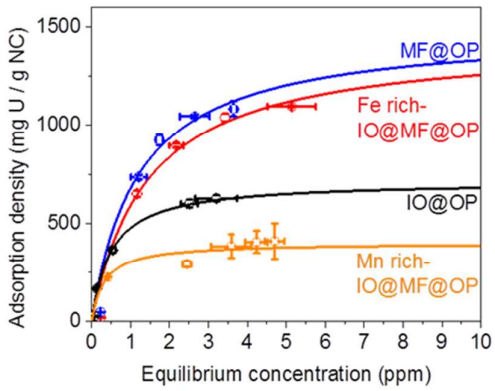

Fig 3. Uranium sorption isotherm of three different types of the nanocrystal samples (MF ([Mn]/[Fe] = 0.30, blue), iron-rich IO@MF ([Mn]/[Fe] = 0.28, red), IO (black), and Mn-rich IO@MF@OP ([Mn]/[Fe] = 2.07, orange)) coated with oleylphosphate (OP) at pH 7.0 for 24 h. The curves were plotted and modeled as Langmuir isotherms.

Surface stabilized IO@MF@OP nanocrystals were evaluated as sorbent materials for uranyl (VI) cations (UO_2^{2+} and hydroxo complexes such as, $(UO_2)_m(OH)_n^{2m-n}$, depending on pH) over varied water chemistries.[18] It should be noted that IO@MF@OP nanocrystals maintained their monodisperse status for U concentration up to 20 ppm (Fig S8); D_H for IO@MF@OP slightly increased from 20 to ca. 35 nm at pH 5.6 and pH 7.0 as U concentration was increased to 40 ppm. Fig 3 shows nanocrystal composition dependent U sorption capacity measurements. Each was modeled as a Langmuir isotherm.[19] Maximum sorption capacity (q_{max}) for IO@MF with an iron rich ferrite shell is similar to values for MF nanocrystals with the same bilayer coatings. q_{max} for IO@MF@OP ([Mn]/[Fe] = 0.28) and manganese ferrites (MF: $Mn_{0.6}Fe_{2.4}O_4$, [Mn]/[Fe] = 0.30) at pH 7.0 was 1438 and 1492 mg of U per g of nanocrystal (mg U / g NC), respectively.[13] U(VI) sorption capacity of IO@MF@OP ([Mn]/[Fe] = 0.28) at pH 5.6 was near the capacity at pH 7.0 (Fig S9). For these, all isotherm modeling data is presented in Table S2. These value are among some of the highest values reported for uranium sorbents.[13, 20]

While iron rich MF coatings can improve U sorption capacities of IO nanocrystals by a factor of two, higher Mn shell content ([Mn]/[Fe] = 2.07), which resulted in Mn-rich MF coatings (with manganese oxide phase shown in via XRD Fig S6), display a marked decrease of U sorption capacity. Fig 3 shows U sorption capacities of IO@MF@OP as a function of Mn to Fe ratios in the shell composition from 0.28 to 2.07 with q_{max} of IO@MF@OP nanocrystals decreasing from 1438 to 400 mg U / g NC, respectively. We hypothesize that the decrease of q_{max} for Mn-rich IO@MF nanocrystal ([Mn]/[Fe] in a nanocrystal was 2.07) is due to the formation of pure manganese oxide phases (and/or manganese-rich ferrite such as, Mn_2FeO_4) on the iron oxide core.[13, 14] It has been previously reported that Mn precursor decomposition with high concentration in the presence of IO seeds (when [Mn] / [Fe] of the starting materials was over 2.1) does form thick layered Mn_2FeO_4, MnO, or Mn_3O_4 on the surface of IO nanocrystals (Fig S6).[13-15] Such (thick) Mn-rich phase layers on IO nanocrystal may prevent high U sorption properties as less reduced Fe (Fe(II)) is available, which is critical for U reduction from U(VI) to U(IV), on the surface of IO-based materials.[13, 21]

For materials exhibiting the highest U sorption capacity ([Mn]/[Fe] in a nanocrystal was 0.28), the relatively highest percentage of U reduction was also observed. Fig 4 shows U reduction as a function of nanocrystal surface composition. The highest U reduction (from U(VI) to U(IV)) was found from Fe-rich IO@MF with U(IV) of 65 %; the U reduction percentage of IO and Mn-rich IO@MF was 58 and 52 %, respectively (Table S3). As mentioned above, we hypothesize that Fe(II) on the surface of the nanocrystal samples play a significant role in U reduction (Fig S9 and Table S4). Fe(II) concentration of Fe-rich IO@MF decreased from 75 % to 25 % upon U reduction; Mn(II) of Fe-rich IO@MF was also observed to decrease from 28 % to 14 % with U reduction experiment (Fig S10, Fig S11, Table S4, and Table S5).

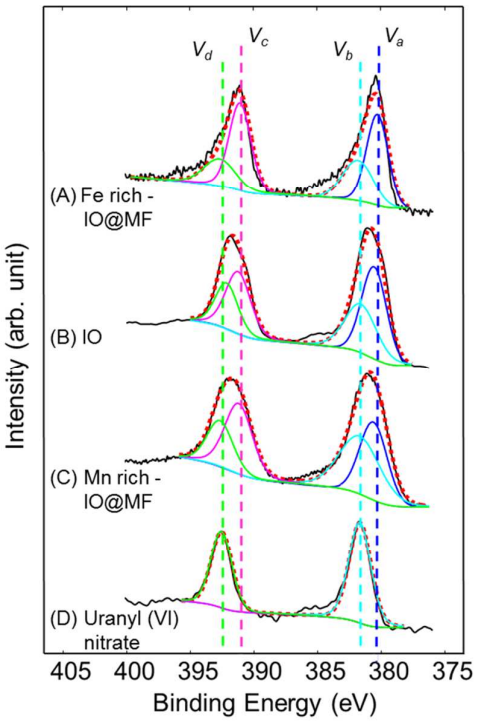

Fig 4. XPS spectra of the uranium (U) 4f spectra for the sample after uranium sorption. The black lines are the raw data and the red dash lines are the fitted curves based on curve fitting using V_a (blue), V_b (sky blue), V_c(pink), and V_d(green). The ratio of U(IV) to U(VI) was calculated by $(V_a+V_b)/(V_c+V_d)$ in the XPS spectra of U4f from the sample after the uranium sorption measurement and compared with uranyl (VI) nitrate.

Conclusions

Surface tunable, superparamagnetic IO@MF nanocrystals coated with phosphate group functionalized bilayer surface coatings are demonstrated to be highly effective for uranium sorption/separation in water. The highest U sorption capacity of IO@MF nanocrystals (q_{max} was 1438mg U / g NC) was found to occur for surface stable IO nanocrystals with an iron-rich MF shell structure ([Mn]/[Fe] of an IO@MF nanocrystal = 0.28) with significant redox reactions at the particle interface. Such capacity is among the highest reported to date. Taken together, these findings underpin broad, platform potential for these and similar materials for next generation water treatment, including actinide separation and sensing technologies.

Conflicts of interest

There are no conflicts to declare.

Acknowledgements

This work is supported by U.S. Army Corps of Engineers (W912HZ-13-2-0009-P00001) and the US National Science Foundation (CBET 1437820). TEM, DLS, ICP-OES, and ICP-MS were provided by the Nano Research Facility (NRF), EFTEM, EDS, XPS, and XRD were provided by the Institute of Materials Science & Engineering (IMSE) at Washington University in St. Louis.

Notes and references

† Electronic Supplementary Information (ESI) available: Supporting Information includes detailed descriptions for the experimental details, CCC, TEM, EDS, XRD, and XPS analysis. See DOI: 10.1039/x0xx00000x

References

1. J. Gomez-Pastora, E. Bringas and I. Ortiz, Recent progress and future challenges on the use of high performance magnetic nano-adsorbents in environmental applications, *Chemical Engineering Journal*, 2014, **256**, 187-204.
2. S. C. N. Tang and I. M. C. Lo, Magnetic nanoparticles: Essential factors for sustainable environmental applications, *Water Research*, 2013, **47**, 2613-2632.
3. X. L. Qu, J. Brame, Q. L. Li and P. J. J. Alvarez, Nanotechnology for a Safe and Sustainable Water Supply: Enabling Integrated Water Treatment and Reuse, *Accounts of Chemical Research*, 2013, **46**, 834-843.
4. G. K. Das, C. S. Bonifacio, J. De Rojas, K. Liu, K. van Benthem and I. M. Kennedy, Ultra-long magnetic nanochains for highly efficient arsenic removal from water, *Journal of Materials Chemistry A*, 2014, **2**, 12974-12981.
5. C. J. Jones, S. Chattopadhyay, N. I. Gonzalez-Pech, C. Avendano, N. N. Hwang, S. S. Lee, M. J. Cho, A. Ozarowski, A. Prakash, J. T. Mayo, C. Yavuz and V. L. Colvin, A Novel, Reactive Green Iron Sulfide (Sulfide Green Rust) Formed on Iron Oxide Nanocrystals, *Chemistry of Materials*, 2015, **27**, 700-707.
6. S. P. Yeap, S. S. Leong, A. L. Ahmad, B. S. Ooi and J. Lim, On Size Fractionation of Iron Oxide Nanoclusters by Low Magnetic Field Gradient, *Journal of Physical Chemistry C*, 2014, **118**, 24042-24054.
7. C. Kim, S. S. Lee, B. J. Lafferty, D. E. Giammar and J. D. Fortner, Engineered superparamagnetic nanomaterials for arsenic (V) and chromium (VI) sorption and separation: quantifying the role of organic surface coatings, *Environmental Science: Nano*, 2018, **5**, 556-563.
8. R. A. Crane, M. Dickinson, I. C. Popescu and T. B. Scott, Magnetite and zero-valent iron nanoparticles for the remediation of uranium contaminated environmental water, *Water Research*, 2011, **45**, 2931-2942.
9. J. N. Dui, G. Y. Zhu and S. M. Zhou, Facile and Economical Synthesis of Large Hollow Ferrites and Their Applications in Adsorption for As(V) and Cr(VI), *Acs Applied Materials & Interfaces*, 2013, **5**, 10081-10089.
10. C. T. Yavuz, J. T. Mayo, W. W. Yu, A. Prakash, J. C. Falkner, S. Yean, L. L. Cong, H. J. Shipley, A. Kan, M. Tomson, D. Natelson and V. L. Colvin, Low-field magnetic separation of monodisperse Fe3O4 nanocrystals, *Science*, 2006, **314**, 964-967.
11. Y. Cai, C. Wu, Z. Liu, L. Zhang, L. Chen, J. Wang, X. Wang, S. Yang and S. Wang, Fabrication of a phosphorylated graphene oxide–chitosan composite for highly effective and selective capture of U (VI), *Environmental Science: Nano*, 2017, **4**, 1876-1886.
12. L. Chen, Z. Bai, L. Zhu, L. Zhang, Y. Cai, Y. Li, W. Liu, Y. Wang, L. Chen and J. Diwu, Ultrafast and Efficient Extraction of Uranium from Seawater Using an Amidoxime Appended Metal–Organic Framework, *ACS applied materials & interfaces*, 2017, **9**, 32446-32451.
13. S. S. Lee, W. Li, C. Kim, M. Cho, B. J. Lafferty and J. D. Fortner, Surface functionalized manganese ferrite nanocrystals for enhanced uranium sorption and separation in water, *Journal of Materials Chemistry A*, 2015, **3**, 21930-21939.
14. K. L. Krycka, J. A. Borchers, G. Salazar-Alvarez, A. Lopez-Ortega, M. Estrader, S. Estrade, E. Winkler, R. D. Zysler, J. Sort, F. Peiro, M. D. Baro, C. C. Kao and J. Nogues, Resolving Material-Specific Structures within Fe_3O_4 vertical bar gamma-Mn_2O_3 Core vertical bar Shell Nanoparticles Using Anomalous Small-Angle X-ray Scattering, *Acs Nano*, 2013, **7**, 921-931.
15. A. Lopez-Ortega, M. Estrader, G. Salazar-Alvarez, S. Estrade, I. V. Golosovsky, R. K. Dumas, D. J. Keavney, M. Vasilakaki, K. N. Trohidou, J. Sort, F. Peiro, S. Surinach, M. D. Baro and J. Nogues, Strongly exchange coupled inverse ferrimagnetic soft/hard, $Mn_xFe_{3-x}O_4/Fe_xMn_{3-x}O_4$, core/shell heterostructured nanoparticles, *Nanoscale*, 2012, **4**, 5138-5147.
16. K. An, M. Park, J. H. Yu, H. B. Na, N. Lee, J. Park, S. H. Choi, I. C. Song, W. K. Moon and T. Hyeon, Synthesis of Uniformly Sized Manganese Oxide Nanocrystals with Various Sizes and Shapes and Characterization of Their T1 Magnetic Resonance Relaxivity, *European Journal of Inorganic Chemistry*, 2012, DOI: DOI 10.1002/ejic.201101193, 2148-2155.
17. A. Prakash, H. G. Zhu, C. J. Jones, D. N. Benoit, A. Z. Ellsworth, E. L. Bryant and V. L. Colvin, Bilayers as Phase Transfer Agents for Nanocrystals Prepared in Nonpolar Solvents, *Acs Nano*, 2009, **3**, 2139-2146.

18. M. Sutton and S. R. Burastero, Uranium(VI) solubility and speciation in simulated elemental human biological fluids, *Chemical Research in Toxicology*, 2004, **17**, 1468-1480.
19. I. Langmuir, The Adsorption of Gases on Plane Surfaces of Glass, Mica and Platinum., *Journal of the American Chemical Society*, 1918, **40**, 1361-1403.
20. E. Calì, J. Qi, O. Preedy, S. Chen, D. Boldrin, W. Branford, L. Vandeperre and M. Ryan, Functionalised magnetic nanoparticles for uranium adsorption with ultra-high capacity and selectivity, *Journal of Materials Chemistry A*, 2018, **6**, 3063-3073.
21. W. Li, L. D. Troyer, S. S. Lee, J. Wu, C. Kim, B. J. Lafferty, J. G. Catalano and J. D. Fortner, Engineering nanoscale iron oxides for uranyl sorption and separation: Optimization of particle core size and bilayer surface coatings, *ACS applied materials & interfaces*, 2017, **9**, 13163-13172.